Journal of Power Sources 296 (2015) 344–351

Contents lists available at ScienceDirect

Journal of Power Sources

journal homepage: www.elsevier.com/locate/jpowsour

Thermal conductivity of microporous layers: Analytical modeling and experimental validation

Mehdi Andisheh-Tadbir [a, b], Erik Kjeang [a], Majid Bahrami [a, *]

[a] Laboratory for Alternative Energy Conversion (LAEC), School of Mechatronic Systems Engineering, Simon Fraser University, Surrey, BC V3T 0A3, Canada
[b] Fuel Cell Research Laboratory (FCReL), School of Mechatronic Systems Engineering, Simon Fraser University, Surrey, BC V3T 0A3, Canada

HIGHLIGHTS

- A compact analytical relationship for the MPL thermal conductivity is developed.
- Transient plane source technique used to measure MPL thermal conductivity.
- Effect of compression on thermal conductivity is investigated.
- A multi objective genetic algorithm is used to find optimal MPL structure.

GRAPHICAL ABSTRACT

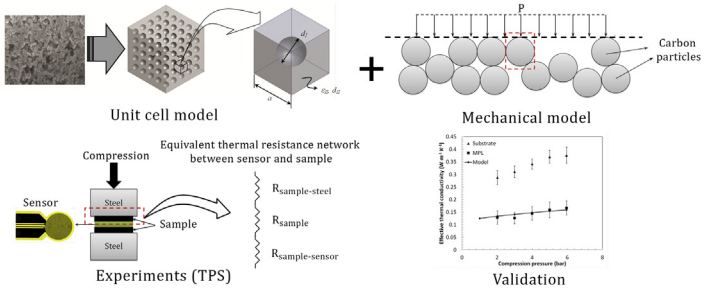

ARTICLE INFO

Article history:
Received 19 May 2015
Received in revised form
14 July 2015
Accepted 17 July 2015
Available online 30 July 2015

Keywords:
Micro-porous layer
Fuel cell
Analytical model
Thermal conductivity
TPS
Pore size distribution

ABSTRACT

A new compact relationship is developed for the thermal conductivity of the microporous layer (MPL) used in polymer electrolyte fuel cells as a function of pore size distribution, porosity, and compression pressure. The proposed model is successfully validated against experimental data obtained from a transient plane source thermal constants analyzer. The thermal conductivities of carbon paper samples with and without MPL were measured as a function of load (1–6 bars) and the MPL thermal conductivity was found between 0.13 and 0.17 W m^{-1} K^{-1}. The proposed analytical model predicts the experimental thermal conductivities within 5%. A correlation generated from the analytical model was used in a multi objective genetic algorithm to predict the pore size distribution and porosity for an MPL with optimized thermal conductivity and mass diffusivity. The results suggest that an optimized MPL, in terms of heat and mass transfer coefficients, has an average pore size of 122 nm and 63% porosity.

1. Introduction

The membrane electrode assembly (MEA) used in polymer electrolyte fuel cells consists of a membrane, two electrodes for the anode and cathode side, and two gas diffusion layers (GDLs). The GDL is responsible for providing the pathways for transport of the reactant gases from the flow channels to the catalyst layers as well as mechanical support for other porous layers in the MEA. GDL is typically a dual-layer carbon-based material composed of a macro-porous substrate, which usually contains carbon fibers, binder, and polytetrafluoroethylene (PTFE), and a thin delicate micro-porous layer (MPL), which is usually made of carbon nano-particles and PTFE.

Apart from the improvements in polymer electrolyte membrane fuel cell (PEMFC) water management [1,2], MPL is known to affect

* Corresponding author.
E-mail addresses: mandishe@sfu.ca (M. Andisheh-Tadbir), ekjeang@sfu.ca (E. Kjeang), mbahrami@sfu.ca (M. Bahrami).

http://dx.doi.org/10.1016/j.jpowsour.2015.07.054
0378-7753/

the electrical/thermal contact resistances between the GDL and catalyst layer [3,4]. This is mainly due to the homogenous and softer structure of MPL that can provide a 'transition region,' filling the gaps between the substrate and catalyst layer. Although the contact resistances might reduce after using MPL, bulk properties of MPL could affect the overall fuel cell performance considerably. Hence, it is necessary to have an in-depth understanding of the factors affecting the effective properties of MPL.

MPL is a recently developed material and few studies focused on this thin layer have been published [5–12]. The authors have proposed an analytical relationship to estimate the effective diffusivity of MPL in Ref. [11]. El Hannach et al. [12] also recently published a novel stochastic tool for reconstruction of the MPL structure and calculation of its properties. Few experimental investigations have focused on MPL effective transport properties, e.g., thermal/electrical conductivity, diffusivity [13–15]. Measuring the MPL thermal conductivity is challenging as MPL needs the physical support of a substrate [14]. Numerical tools utilizing 3D FIB/SEM reconstructions of MPL are being used to model MPL properties [13,16]. These numerical models, while experimentally validated, are complex and require significant computational resources to reconstruct the structure, and to solve the governing equations. In most cases, only a small portion ($1–2\ \mu m^3$) of the material is reconstructed and modeled [12,13]. Although numerical models provide accurate results, it is advantageous to have an analytical relationship that correlates design parameters to the MPL thermal conductivity to reduce the computational costs.

In this investigation, a unit cell approach is used to analytically model the thermal conductivity of porous MPL. A unit cell is a simple geometry that inherits the most important specifications of a porous medium and represents the entire medium structure. Our colleagues in Refs. [4,17] utilized this approach to model the thermal conductivity of GDL substrate successfully. To the best knowledge of the authors, there is no relationship available in the literature for estimation of MPL thermal conductivity based on its structure. Existing relationships for the effective properties of porous materials [18–22], have not been specifically developed for MPL and do not produce accurate values for MPL properties.

The present study proposes a new compact relationship to accurately calculate the effective thermal conductivity of MPL as a function of pore size distribution and porosity. The relationship between the structure of the MPL and its heat and mass transport coefficients is explored and the best design point is chosen from the pool of optimal designs obtained from multi objective genetic algorithm based on a criterion which will be explained in the manuscript. Moreover, the present model is suitable for implementation in complex performance models that require an accurate estimation of the effective transport properties with less computational cost.

2. Modeling approach

This work is a continuation of our published model [11]. Here we utilize the same unit cell model, which was used for diffusivity modeling, to model the MPL thermal conductivity. Unlike the mass diffusion coefficient estimation that only considers the mass transport through the gas phase domain, for the thermal conductivity estimation, the heat conduction through the solid structure plays an important role. The considered unit cell is shown in Fig. 1. The unit cell consists of a spherical pore (domain I) inside a porous cube (domain II); details on obtaining the geometrical model parameters from the pore size distribution can be found in Ref. [11]. The required equation for calculating the effective thermal conductivity for such geometry is [23]:

$$k_{eff} = \frac{3k_{II}k_I\alpha + (2k_{II} + k_I)k_{II}(1-\alpha)}{3k_{II}\alpha + (2k_{II} + k_I)(1-\alpha)} \tag{1}$$

where, k_I and k_{II} are the thermal conductivities for the domains *I* and *II*, *c.f.* Fig. 1; and α is the ratio of sphere volume to the total cube volume and is calculated from Eq. (2), in which a is the unit cell dimension as shown in Fig. 1.

$$\alpha = \frac{\pi}{6}\left(\frac{d_I}{a}\right)^3 \tag{2}$$

The spherical pore, domain *I*, only contains stagnant gas, with thermal conductivity k_I. The pores are small ($d_I < 300$ nm) and bulk thermal conductivity of the gas needs to be modified to include the rarefied gas or Knudsen regime effects. In Knudsen regimes, the gas thermal conductivity is a function of pore diameter in which the gas is stored. Kaganer [24] proposed the following relationship to approximate the gas thermal conductivity as a function of pore size.

$$k_I = \frac{k_{g,0}}{1 + 2\beta\frac{\lambda}{d_I}} \tag{3}$$

where $k_{g,0}$ is the gas thermal conductivity at standard conditions when Knudsen number is sufficiently small and the regime is continuum. The coefficient β is a parameter that is calculated from the gas accommodation coefficient, α_T, and the specific heat ratio of gas, γ.

$$\beta = \left(\frac{9\gamma - 5}{2\gamma + 1}\right)\left(\frac{2 - \alpha_T}{\alpha_T}\right) \tag{4}$$

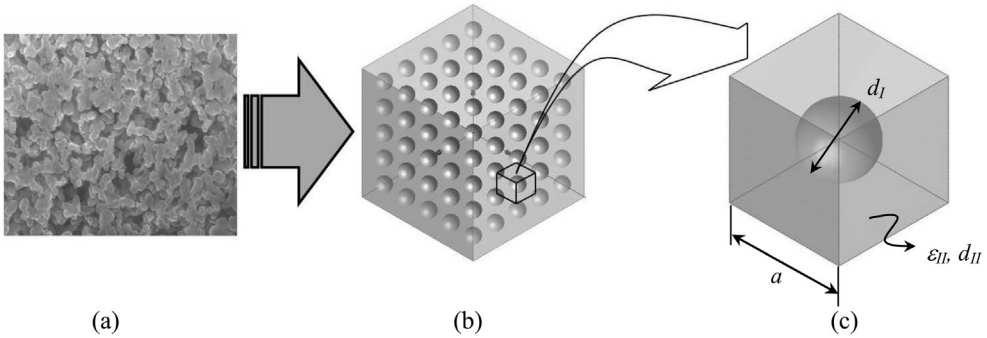

Fig. 1. (a) SEM image from MPL cross section; (b) simplified geometry of the MPL based on unit cell approach; (c) considered unit cell in the present model, d_I is diameter of the sphere, i.e., domain I, and d_{II} is the pore size for domain II.

There is a complicated relationship for the gas accommodation coefficient [25], but α_T is 0.7–1.0 for common gases at room temperature [26]. For air at 25 °C, γ is 1.4, α_T is 0.8, β is ~3 [26] and the mean free path, λ, is 68 nm [27].

Domain *II*, the MPL porous packed bed of spherical carbon nanoparticles, has a thermal conductivity, k_{II}, that can be approximated using the equation of Hsu et al. for a packed bed of spheres [28], which here, it is modified to include the gas rarefaction effects.

$$k_{II} = \left(1 - \frac{1}{\sqrt{1-\varepsilon_{II}}}\right) \frac{k_{g,0}}{1 + 6\frac{\lambda}{d_{II}}} + \left(\frac{1 - r_s^2}{\sqrt{1-\varepsilon_{II}}}\right) k_{gs} + \left(\frac{r_s^2}{\sqrt{1-\varepsilon_{II}}}\right) k_s \tag{5}$$

In Eq. (5), the first term is the thermal conductance of the gas stored in domain II pores with diameter d_{II}, the second term is the equivalent conductance of a mixed gas–solid region, and the third term is the conductance of the solid phase. Parameter k_s is the solid phase thermal conductivity (carbon-PTFE), and r_s is the dimensionless contact radius. Here, the effect of PTFE is considered by assuming an effective value for k_s based on the mass fraction of PTFE. This might not be the most accurate approach to include the effect of PTFE on thermal conductivity; however, it is the least complex method. It is shown in Ref. [15], that the PTFE content is affecting the MPL thermal conductivity significantly; however, PTFE distribution in the MPL structure can influence the overall MPL thermal conductivity.

$$r_s^2 = 1 - \frac{1}{(1+\omega B)^2} \tag{6}$$

In Eq. (6), B is the particle shape factor and ω is the deformed factor, which dictates the amount of contact area between the particles.

According to the Hertzian theory [29], the radius of the contact area between two identical spheres, η, under compression has the following relationship with the applied force, F.

$$\eta = \left(\frac{3FR}{8E^*}\right)^{1/3} \tag{7}$$

where R is the effective radius, and E^* is the effective modulus of elasticity that can be found from the Poisson's ratio, ν, and the elastic modulus, E, of carbon.

$$\frac{1}{E^*} = 2\frac{1-\nu^2}{E} \tag{8}$$

Fig. 2 shows a free body diagram of a layer of MPL in which the area of particles in contact with the compression plane is determined from the solid fraction of MPL. Therefore, the amount of force exerted on each particle is $F = 4PR^2/1 - \varepsilon_{MPL}$. Substituting this in Eq. (7), the final relationship for calculating the contact radius is found as a function of compression pressure.

$$\eta = R\left(\frac{3P}{2(1-\varepsilon_{MPL})E^*}\right)^{1/3} \tag{9}$$

Equating dimensionless contact radius, η/R, to Eq. (6), the equation for the deformed factor, ω is:

$$\omega = \frac{1}{B}\sqrt{\frac{1}{1 - \left(\frac{3P}{2(1-\varepsilon_{MPL})E^*}\right)^{2/3}}} - \frac{1}{B} \tag{10}$$

The equivalent conductance of the mixed solid–gas can be calculated from Eq. (11).

$$\frac{k_{gs}}{k_g} = \frac{2}{1-\xi B + (1-\xi)\omega B}\left(\frac{(1-\xi)(1+\omega)B(1+\omega B)^2}{[1-\xi B + (1-\xi)\omega B]^2}\ln\left(\frac{1+\omega B}{(1+\omega)B\xi}\right) - \frac{B+1+2\omega B}{2} - \frac{(B-1)(1+\omega B)}{1-\xi B + (1-\xi)\omega B}\right) \tag{11}$$

where ξ is the ratio of gas to solid conductivity, and the shape factor, B, is calculated as follows [28].

$$B = 1.25\left(\frac{1-\varepsilon_{II}}{\varepsilon_{II}}\right)^{1.11} \tag{12}$$

ε_{II} is the domain *II* porosity, which can be found as a function of the MPL porosity and pore size distribution, using Eq. (13) [11].

$$\varepsilon_{II} = \frac{(d_I - d_{avg})\varepsilon_{MPL}}{(d_{II} - d_{avg})\varepsilon_{MPL} + d_I - d_{II}} \tag{13}$$

The unit cell size is [11]:

$$a = d_I\left(\frac{\pi}{6\left(1 - \frac{1-\varepsilon_{MPL}}{1-\varepsilon_{II}}\right)}\right)^{\frac{1}{3}} \tag{14}$$

To calculate the thermal conductivity of MPL, the porosity and pore size distribution of the MPL are used to generate the geometrical parameters of the model, i.e., d_I, d_{II}, and d_{avg}, as explained in our previous paper [11]. The sequence of calculations is depicted in Fig. 3.

3. Experimental study

3.1. Sample specifications

Measurement of MPL properties is challenging because MPL is not available as a stand-alone layer. In this study, the microporous layer of SIGRACET® GDL is selected for measurement and model validation purposes. GDLs 24 BA and 34 BA have different thicknesses but almost identical structure and porosity. The MPL coated versions of these substrates, SGL 24 BC and 34 BC, have 45 and 35 μm MPL layers, respectively. Specifications of the samples used in this work are listed in Table 1.

3.2. Thermal conductivity measurements

A thermal constants analyzer (TPS 2500S, ThermTest Inc., Fredericton, Canada) capable of precise measurement of thermal conductivity, diffusivity and specific heat was used for this study. The instrument has different sensor types and software modules to

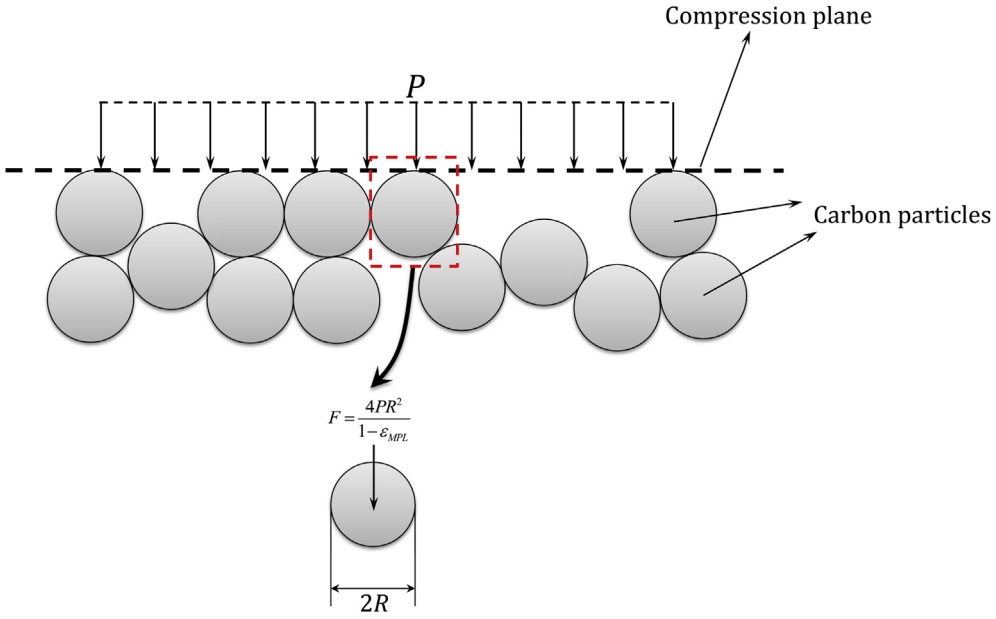

Fig. 2. Schematic of the carbon particles of the porous MPL under compression.

perform measurements on bulk materials (isotropic and anisotropic), thin films, powders and liquids. This machine uses the transient plane source method and theory in accordance with ISO Standard 22007-2. In this work, a thin film sensor (7280) with a 29.4 mm diameter nickel double spiral insulated in a thin layer of Kapton is used for both transient heating of the sample and precise temperature measurements.

For thin film measurements, a pair of identical samples are placed on either side of the sensor and compressed between two smooth stainless steel blocks. After 20 min for temperature equilibration, measurements are performed on each sample at different compression pressures between 1 and 6 bars. The sample-sensor assembly and the corresponding equivalent thermal resistance network including the contact resistances between the sample and sensor and the sample and steel are shown in Fig. 4. The power from the heat source, $\dot{Q}$, the temperature rise between the sensor and steel block, ΔT, the sensor area, A, and the sample thickness, t_{sample}, are used to calculate the apparent sample thermal conductivity.

$$k_{sample} = \frac{\dot{Q}}{A}\frac{\Delta T}{t_{sample}} \tag{15}$$

Contact resistances are included in this measured apparent thermal conductivity and can be significant, especially for porous, rough or rigid thin materials with air gaps between the sensor and sample. Therefore, for accurate values for the thermal conductivity it is needed to remove those effects.

3.2.1. Removing the contact resistance effects

To determine the k_{eff}, the total resistance, $R_{tot} = t_{sample}/k_{tot}$, is calculated, in which k_{tot} is the uncorrected value of the thermal conductivity which is reported by the TPS software. The corrected thermal conductivity value, k_{eff}, should be found after removing the contact resistance effects following the two thickness method [4].

$$R_{tot} = R_{sample} + R_c, \quad R_{sample} = \frac{t_{sample}}{k_{eff}} \tag{16}$$

By measuring the resistance for two different thicknesses of the same material, it is possible to calculate k_{eff} and R_c, the two unknowns in two measurements.

$$k_{eff} = \frac{t_{sample,2} - t_{sample,1}}{R_{tot,2} - R_{tot,1}}, \quad R_c = R_{tot,1} - \frac{t_{sample,1}}{k_{eff}} \tag{17}$$

For each GDL type, five pairs of 4 × 4 cm^2 samples were prepared. The thermal conductivity of each pair of samples was measured three times with a rest interval of ten minutes between measurements.

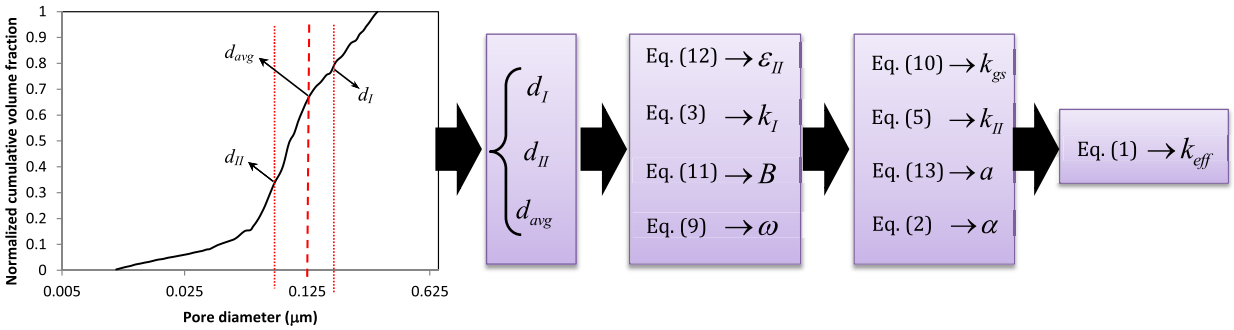

Fig. 3. Steps to calculate thermal conductivity using the proposed model.

Table 1
Specifications of SIGRACET® samples used in the present study.[a]

	Porosity (%)	Substrate thickness (μm)	MPL thickness (μm)
SGL 24 BA	84	190	–
SGL 24 BC	76	235	45
SGL 34 BA	83	280	–
SGL 34 BC	75	315	35

[a] Reported by SGL Group with inter-lot intra-lot homogeneity of less than ±10% [30,31].

3.3. Thickness measurements

The thickness of GDLs under compression load was measured by a custom-made tool at Ballard Power Systems. GDL samples of each type were prepared with a circular punch (24.5 mm). Thickness measurements with accuracy of ±1 μm were made with loads from 1 to 6 bar. The MPL thickness is calculated by subtracting the thickness of the BC type GDL from the corresponding BA type GDL.

4. Results

Thermal resistance network for a GDL sample that has MPL includes the MPL resistance, the substrate resistance, and the contact resistance between these two layers. Subtracting the total resistances for two GDLs that has MPLs with different thicknesses, result in omitting that interfacial resistance, by assuming the interfacial resistances are identical due to the similarities in microstructures. Therefore, the MPL thermal conductivity can be calculated from the following equation.

$$k_{MPL} = \frac{t_{MPL,24BC} - t_{MPL,34BC}}{(R_{34BC,tot} - R_{34BC,sub}) - (R_{24BC,tot} - R_{24BC,sub})}$$
$$R_{24BC,sub} = \frac{t_{24BC,sub}}{k_{sub}}, \quad R_{34BC,sub} = \frac{t_{34BC,sub}}{k_{sub}} \tag{18}$$

In Eq. (18), $t_{MPL,24BC}$ and $t_{MPL,34BC}$ are the MPL thicknesses for the 24 BC and 34 BC GDLs; $R_{24BC,tot}$ and $R_{34BC,tot}$ are the total resistances of SGL 24 BC and 34 BC; and $R_{24BC,sub}$ and $R_{34BC,sub}$ are the thermal resistances of the substrate for the SGL 24 BC and 34 BC.

4.1. GDL thicknesses and total resistances

The changes in the GDL thickness under compression for various GDL types are plotted in Fig. 5(a). Note that the overall GDL thickness reduces up to 5% with the applied compression.

Fig. 5(b) presents the total measured resistances for the four GDL types at various compression pressures. The uncertainty of the total resistance measurements, including the standard deviation of the apparent thermal conductivity measurements, was less than 2% for all sample types. The error bars are less than the height of the markers used for data in the plot. These resistances include the contact resistances, which their effects should be removed to obtain the effective thermal conductivities. As mentioned in Section 3.1, thermal conductivity of SGL 24 BA and 34 BA are identical; and its corresponding value can be calculated from Eq. (18).

4.2. Effective thermal conductivity of MPL

Fig. 6 shows the effective MPL thermal conductivity obtained from Eq. (18). The measured values for the substrate thermal conductivity are consistent with the reported values for the same GDL, i.e., SGL 24 BA, in Ref. [4]. However, there is a discrepancy between the obtained MPL thermal conductivity values in this work and tests conducted by our colleagues using a different apparatus [4]. The average uncertainty of measurements is less than 8% for the GDL substrate and is less than 18% for MPL. The uncertainty analysis is discussed in Appendix A.

The MPL model results are plotted in Fig. 6. The model predicts the thermal conductivity values as a function of pressure with a good accuracy within the uncertainty of the measurements. While the substrate shows a stronger dependence on compression, a slight functionality of pressure is observed for MPL. The same slope of the thickness–compression curve for samples with and without MPL shows that the majority of the thickness changes occur in the substrate, *c.f.* Fig. 5. Hence, one may conclude that due to the slight changes in the structure of MPL up to 6 bar, there is no significant alteration of thermal conductivity. However, this statement is not valid for the substrate that exhibited a sizable deformation under compression, and therefore a steeper thermal conductivity–pressure curve.

4.3. Compact relationship development

The analytical model was used to generate over 200 values for MPL thermal conductivity as a function of d_I, d_{II}, d_{avg}, and porosity. For the generated points, the range of pore size varied between 80 and 150 nm for d_I, d_{II}, d_{avg}, and porosity was kept between 0.4 and 0.6. A compact relationship between thermal conductivity and these parameters was developed that provides an estimation of the MPL thermal conductivity with less than 10% deviation from the predicted value by Eq. (1).

If all parameters are substituted in Eq. (1), it can be seen that $d_I - d_{avg}/d_{avg} - d_{II}$ is a suitable candidate for selection as a dimensionless characteristic pore size. Hence, it is chosen as one of the

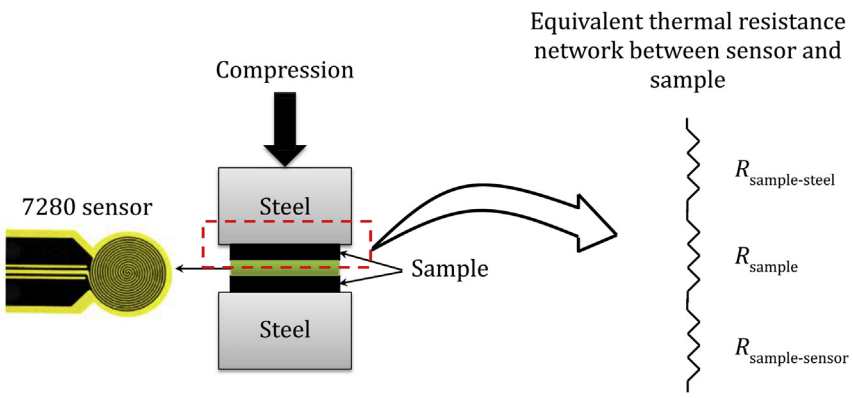

Fig. 4. Schematic of the sample arrangement in TPS 2500S and the equivalent thermal resistance network.

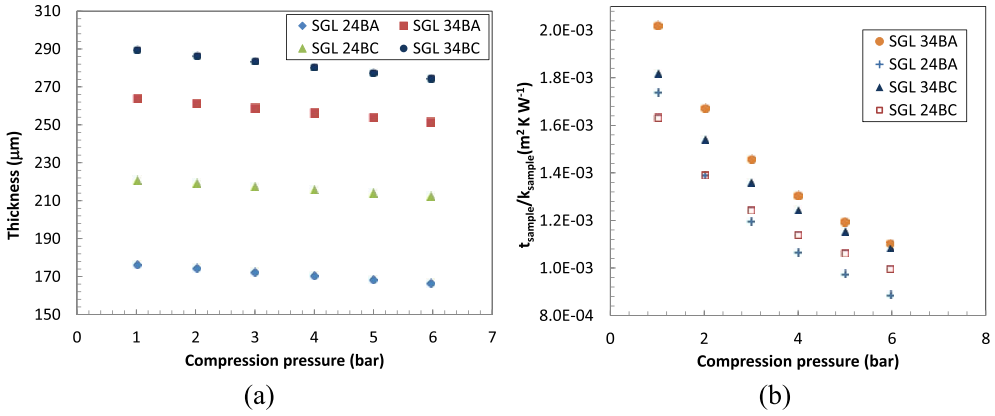

Fig. 5. (a) Variations of thickness under compression for different GDL types; and (b) total thermal resistance calculated from the raw data from TPS 2500S.

independent variables of the correlation. Denoting this parameter by d^*, the effective thermal conductivity would be only a function of d^*, ε_{MPL}, and compression pressure, i.e., $k_{eff}=f(d^*,\varepsilon_{MPL},P)$. LAB Fit software [30] is used to find the best fit on the data out of 572 equations. The best fit to the data is shown in Eq. (19).

$$k_{eff} = \left(3\times10^{-7}P + 0.90\right)\left(-10.76\varepsilon_{MPL}^{-1+0.003/d^*} + \frac{10.77}{\varepsilon_{MPL}}\right) \tag{19}$$

The variations of thermal conductivity versus porosity for several d^* values at 1 bar compression are shown in Fig. 7. The thermal conductivity is higher for lower porosities, i.e., materials with higher solid fraction and fewer air gaps. Therefore, the overall thermal conductivity is higher for low porosity MPLs, which is desirable; however, it is shown in our previous investigation [11] that mass diffusion coefficient decreases as the porosity decreases. Hence, there should be optimal conditions, where both mass diffusivity and thermal conductivity are high. In Section 4.4, specifications for an optimal MPL structure are proposed to get the maximum thermal conductivity and diffusivity.

4.4. Optimal MPL structure for enhanced heat and mass transfer

Better performance of fuel cells will not be achieved unless their components are designed optimally. In this section, a multi objective genetic algorithm ("gamultiobj" in MATLAB [35]) is used to find the optimal structural specifications of the MPL for the maximized effective thermal conductivity and diffusivity. The objective functions for the genetic algorithm are Eq. (19) and the relationship for diffusivity in Ref. [11]. The design variables are $\{d_I, d_{II}, d_{avg}, \varepsilon_{MPL}\}$ and the lower and upper bounds for these variables are set as {100 nm, 40 nm, 90 nm, 0.45} and {200 nm, 80 nm, 150 nm, 0.65}, respectively. The genetic algorithm parameters, e.g., mutation and cross over, are left at their default values.

Fig. 8 presents the effective diffusivity and thermal conductivity at optimal design points. Each of the points in this figure corresponds to local maximum values for the diffusivity and thermal conductivity. Based on an arbitrary criterion chosen by the authors ($k_{eff}>0.2$ and $D>0.1$), the yellow shaded area in Fig. 8 shows the high diffusivity region, and the blue shaded area shows the high thermal conductivity region. The corresponding limiting current density for $D>0.1$ is calculated to be higher than 1.4 A cm^{-2} by assuming purely gas diffusion inside the MEA by using Eq. (20). In Eq. (20) D_{eff} represents the effective diffusivity of the entire cathode electrode (entire GDL and catalyst layer), and C_∞ is the oxygen concentration in the cathode channel. The temperature gradient at this current density can also be obtained from 1D heat conduction assumption. At 1.4 A cm^{-2} the obtained temperature drop along the MPL thickness is 2.3 K for the MPL effective thermal conductivity of 0.2 W m^{-1} K^{-1} and 4.6 K for 0.1 W m^{-1} K^{-1}. To have less

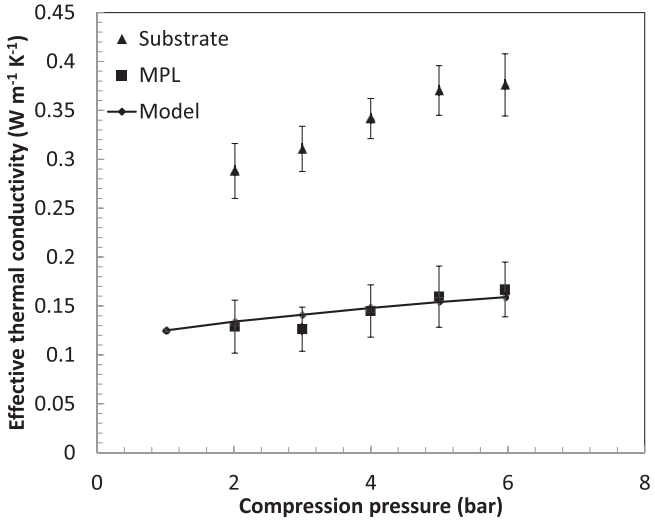

Fig. 6. The measured thermal conductivity of the substrate (▲) and MPL (■), and the MPL thermal conductivity predicted by the present analytical model (line).

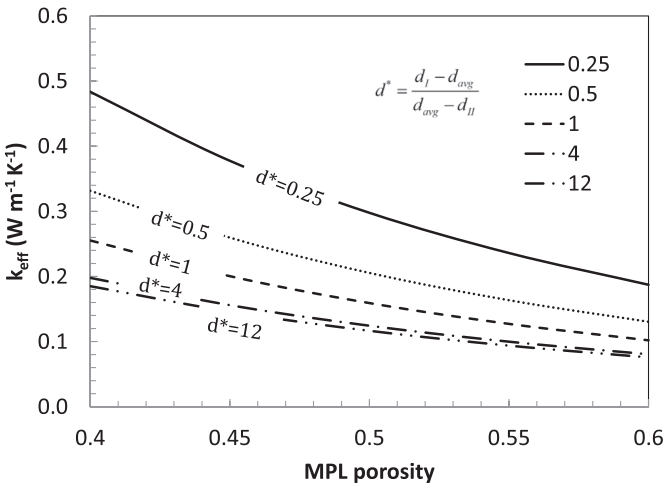

Fig. 7. Variations of thermal conductivity at various d* and porosity values.

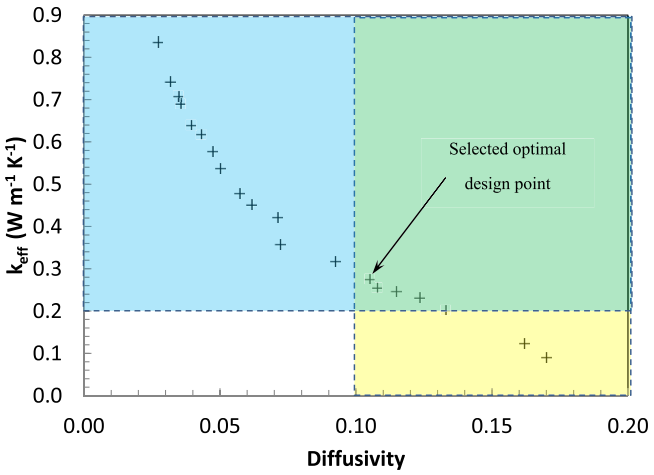

Fig. 8. Effective diffusivity and thermal conductivity at optimal design points.

temperature gradient, it is preferred to choose the thermal conductivities higher than 0.2 for the optimal MPL conditions. The green area presents the region where both diffusivity and thermal conductivity are high. Therefore, the only design point within this region is selected as the optimal design point. The specifications of this design point, which is the optimal MPL structural properties, are listed in Table 2.

$$i_L = nFD_{eff}\frac{C_\infty}{\delta} \tag{20}$$

This data reveals that the MPL structure should have large pores in between dense agglomerates of carbon; the large pores acts as the mass transport pathways, while the dense agglomerates provides the heat transfer pathways.

5. Conclusions

In the present study, a new analytical model was developed to estimate the effective thermal conductivity of MPL as a function of pore size distribution, porosity, and compression pressure. A series of experiments were performed to obtain the MPL thermal conductivity at various pressures. The changes in the thickness of the GDLs due to compression were also measured. The effects of the contact resistances between the samples and the sensor in the apparatus were removed using four GDL types. The measured thermal conductivity values for the MPL under 1–6 bar compression fell between 0.13 and 0.17 W m^{-1} K^{-1} with less than 18% measurement uncertainty. The observed changes in thermal conductivity due to compression were more pronounced in the substrate and only a slight increase in the MPL thermal conductivity was observed as a result of compression.

The model results were validated against experimental data and a compact correlation was proposed based on more than 200 thermal conductivity values generated by the analytical model. The obtained correlation for the MPL thermal conductivity and the diffusivity were used in a multi objective function to suggest an optimal MPL structure.

Table 2
Specifications of an optimal MPL design.

d_I(nm)	d_{II}(nm)	d_{avg}(nm)	ε_{MPL}(%)	k_{eff}(Wm^{-1} K^{-1})	$D_{eff}=\frac{D}{D^0_{O_2}}$
128	71	122	63	0.28	0.11

The following highlights the findings of this work:

- A new analytical relationship was developed for the MPL thermal conductivity as a function of pore size distribution, porosity, and compression pressure.
- MPL thermal conductivity was measured using transient plane source technique at various compression pressures, where effects of contact resistance on the TPS data were removed.
- A compact relationship was proposed to estimate the MPL thermal conductivity.
- A multi objective genetic algorithm was used to find an optimal MPL structure that operate optimally for mass and heat transfer.

Acknowledgments

The authors gratefully acknowledge the financial support from the Natural Sciences and Engineering Research Council of Canada. The first author would also like to thank Dr. Claire McCague for her kind helps in preparing the article.

Appendix A

Eqs. (17) and (18) are the final relationships used for calculating the substrate and MPL thermal conductivities from the measured thermal resistances by the TPS 2500S. Uncertainty in function q that has several variables can be obtained using the following formula, in which δi is the error associated with variable i [31].

$$\delta q = \sqrt{\left(\frac{\partial q}{\partial x}\delta x\right)^2 + \cdots + \left(\frac{\partial q}{\partial z}\delta z\right)^2} \tag{21}$$

Implementing this approach to calculate the uncertainties, the average error for the substrate thermal conductivity is found to be 8%. However, considering the error propagation due to the several mathematical operations on the obtained data, the average uncertainty of MPL thermal conductivity is 18%. Note that this is the maximum error, which is so pessimistic. The other thermal conductivity values reported by other researchers neither do have error bars nor show a lower uncertainty [4,15,32]. For instance in Ref. [32], the authors reported a range for the MPL thermal conductivity due to the uncertainties in measuremen ts; and there is no error bar for the MPL data in Refs. [4,15]. To the knowledge of authors, apart from Refs. [4,15,32], there are no other experimental data available for the MPL thermal conductivity.

Nomenclature

a	unit cell dimension, m
A	area, m^2
B	shape factor, Eq. (12)
C_∞	Oxygen concentration, Eq. (20)
d	diameter, m
D	diffusion coefficient, m^2 s^{-1}
E	modulus of elasticity, 220 GPa
F	force, N
k	thermal conductivity W m^{-1} K^{-1}
P	compression pressure, Pa
Q	heat transfer rate, W
R	thermal resistance, K W^{-1}, and radius of carbon particle, m
r_s	dimensionless contact radius, Eq. (6)
t	thickness, m
TCR	Thermal contact resistance, K W^{-1}

Greek Symbols

α	volume fraction of sphere in the medium, Eq. (2)
α_T	accommodation coefficient
β	model coefficient obtained from Eq. (4)
ΔT	temperature difference, K
ε	porosity
η	contact radius, m
γ	specific heats ratio
ξ	gas to solid thermal conductivity ratio
λ	mean free path, m
ν	Poisson's ratio, 0.3
ω	deformed factor, Eq. (9)

Subscripts

c	contact
I	primary
II	secondary
L	limiting
tot	total
avg	average
eff	effective
s	solid
sub	substrate
g	gas
gs	gas–solid

References

[1] U. Pasaogullari, C.Y. Wang, K.S. Chen, Two-phase transport in polymer electrolyte fuel cells with bilayer cathode gas diffusion media, J. Electrochem. Soc. 152 (2005) A1574.

[2] A.Z. Weber, J. Newman, Effects of microporous layers in polymer electrolyte fuel cells, J. Electrochem. Soc. 152 (2005) A677.

[3] M.M. Mench, E.C. Kumbur, T.N. Veziroglu, E.C. Kumbar, N. Veziroglu, Polymer Electrolyte Fuel Cell Degradation, Elsevier, Academic Press, Oxford, 2012.

[4] H. Sadeghifar, N. Djilali, M. Bahrami, Effect of Polytetrafluoroethylene (PTFE) and micro porous layer (MPL) on thermal conductivity of fuel cell gas diffusion layers: modeling and experiments, J. Power Sour. 248 (2014) 632–641.

[5] W.M. Yan, D.K. Wu, X.D. Wang, A.L. Ong, D.J. Lee, A. Su, Optimal microporous layer for proton exchange membrane fuel cell, J. Power Sour. 195 (2010) 5731–5734.

[6] D. Spernjak, J. Fairweather, R. Mukundan, T. Rockward, R.L. Borup, Influence of the microporous layer on carbon corrosion in the catalyst layer of a polymer electrolyte membrane fuel cell, J. Power Sour. 214 (2012) 386–398.

[7] J.H. Chun, K.T. Park, D.H. Jo, J.Y. Lee, S.G. Kim, S.H. Park, et al., Development of a novel hydrophobic/hydrophilic double micro porous layer for use in a cathode gas diffusion layer in PEMFC, Int. J. Hydrogen Energy 36 (2011) 8422–8428.

[8] R. Schweiss, M. Steeb, P.M. Wilde, T. Schubert, Enhancement of proton exchange membrane fuel cell performance by doping microporous layers of gas diffusion layers with multiwall carbon nanotubes, J. Power Sour. 220 (2012) 79–83.

[9] T. Kitahara, T. Konomi, H. Nakajima, Microporous layer coated gas diffusion layers for enhanced performance of polymer electrolyte fuel cells, J. Power Sour. 195 (2010) 2202–2211.

[10] P. Gallo Stampino, C. Cristiani, G. Dotelli, L. Omati, L. Zampori, R. Pelosato, et al., Effect of different substrates, inks composition and rheology on coating deposition of microporous layer (MPL) for PEM-FCs, Catal. Today 147 (2009) S30–S35.

[11] M. Andisheh-Tadbir, M. El Hannach, E. Kjeang, M. Bahrami, An analytical relationship for calculating the effective diffusivity of micro-porous layers, Int. J. Hydrogen Energy 40 (2015) 10242–10250.

[12] M. El Hannach, R. Singh, N. Djilali, E. Kjeang, Micro-porous layer stochastic reconstruction and transport parameter determination, J. Power Sour. 282 (2015) 58–64.

[13] A. Nanjundappa, A.S. Alavijeh, M. El Hannach, D. Harvey, E. Kjeang, A customized framework for 3-D morphological characterization of micro-porous layers, Electrochim. Acta 110 (2013) 349–357.

[14] C. Chan, N. Zamel, X. Li, J. Shen, Experimental measurement of effective diffusion coefficient of gas diffusion layer/microporous layer in PEM fuel cells, Electrochim. Acta 65 (2012) 13–21.

[15] O.S. Burheim, H. Su, S. Pasupathi, J.G. Pharoah, B.G. Pollet, Thermal conductivity and temperature profiles of the micro porous layers used for the polymer electrolyte membrane fuel cell, Int. J. Hydrogen Energy 38 (2013) 8437–8447.

[16] H. Ostadi, P. Rama, Y. Liu, R. Chen, X.X. Zhang, K. Jiang, 3D reconstruction of a gas diffusion layer and a microporous layer, J. Memb. Sci. 351 (2010) 69–74.

[17] H. Sadeghifar, M. Bahrami, N. Djilali, A statistically-based thermal conductivity model for fuel cell gas diffusion layers, J. Power Sour. 233 (2013) 369–379.

[18] D.A.G. Bruggeman, Calculation of various physics constants in heterogenous substances I dielectricity constants and conductivity of mixed bodies from isotropic substances, Ann. Der. Phys. 24 (1935) 636–664.

[19] G.H. Neale, W.K. Nader, Prediction of transport processes within porous media: diffusive flow processes within a homogeneous swarm of spherical particles, AIChE J. 19 (1973) 112–119.

[20] M.M. Mezedur, M. Kaviany, W. Moore, Effect of pore structure, randomness and size on effective mass diffusivity, AIChE J. 48 (2002) 15–24.

[21] M.M. Tomadakis, S.V. Sotirchos, Ordinary and transition regime diffusion in random fiber structures, AIChE J. 39 (1993) 397–412.

[22] N. Zamel, X. Li, J. Shen, Correlation for the effective gas diffusion coefficient in carbon paper diffusion media, Energy Fuels 23 (2009) 6070–6078.

[23] H.S. Carslaw, J.C. Jaeger, Conduction of Heat in Solids, second ed., Oxford University Press, London, 1959.

[24] M.G. Kaganer, Thermal Insulation in Cryogenic Engineering, Israel Program for Scientific Translation, 1969.

[25] M. Bahrami, M.M. Yovanovich, J.R. Culham, Thermal joint resistances of conforming rough surfaces with gas-filled gaps, J. Thermophys. Heat. Transf. 18 (2004).

[26] J.-S. Kwon, C.H. Jang, H. Jung, T.-H. Song, Effective thermal conductivity of various filling materials for vacuum insulation panels, Int. J. Heat. Mass Transf. 52 (2009) 5525–5532.

[27] S.G. Jennings, The mean free path in air, J. Aerosol. Sci. 19 (1988) 159–166.

[28] C.T. Hsu, P. Cheng, K.W. Wong, Modified Zehner–Schlunder models for stagnant thermal conductivity of porous media, Int. J. Heat. Mass Transf. 37 (1994) 2751–2759.

[29] K.L. Johnson, Contact Mechanics, Cambridge University Press, 1985.

[30] W.P. Silvia, C.M.D.P. Silvia, LAB Fit Curve Fitting Software (Nonlinear Regression and Treatment of Data Program), 2015.

[31] J.R. Taylor, An Introduction to Error Analysis, second ed., University Science Books, 1997.

[32] G. Unsworth, N. Zamel, X. Li, Through-plane thermal conductivity of the microporous layer in a polymer electrolyte membrane fuel cell, Int. J. Hydrogen Energy 37 (2012) 5161–5169.

[35] MATLAB and Statistics Toolbox Release, The MathWorks, Inc., Natick, Massachusetts, United States, 2012b.